HHS Public Access

Author manuscript

Cancer Res. Author manuscript; available in PMC 2021 September 01.

Published in final edited form as:

Cancer Res. 2021 March 01; 81(5): 1216–1229. doi:10.1158/0008-5472.CAN-20-0652.

A transcriptional regulatory loop of master regulator transcription factors, PPARG, and fatty acid synthesis promotes esophageal adenocarcinoma

Sai Ma[1,2,†], **Bo Zhou**[3,†], **Qian Yang**[2,†], **Yunzhi Pan**[4,†], **Wei Yang**[3], **Stephen J. Freedland**[5], **Ling-Wen Ding**[6], **Michael R. Freeman**[3], **Joshua J. Breunig**[7], **Neil A. Bhowmick**[2], **Jian Pan**[8,*], **H. Phillip Koeffler**[2,6], **De-Chen Lin**[2,*]

[1]Department of laboratory, The Affiliated Suzhou Hospital of Nanjing Medical University, Suzhou, China

[2]Department of Medicine, Samuel Ochin Comprehensive Cancer Institute, Cedars-Sinai Medical Center, Los Angeles, USA

[3]Departments of Surgery and Biomedical Sciences, Cedars-Sinai Medical Center, Los Angeles, USA

[4]Department of Pharmacy, The Affiliated Infectious Diseases Hospital of Soochow University, Suzhou, China

[5]Division of Urology, Department of Surgery, Cedars-Sinai Medical Center, Los Angeles, USA and the Durham VA Medical Center, Durham NC, USA

[6]Department of Pathology, Yong Loo Lin School of Medicine, National University of Singapore, Singapore

[7]Board of Governors Regenerative Medicine Institute and Department of Biomedical Sciences, Cedars-Sinai Medical Center, Los Angeles, CA

[8]Department of Hematology and Oncology, Children's Hospital of Soochow University, Suzhou, China

Abstract

Although obesity is one of the strongest risk factors for esophageal adenocarcinoma (EAC), the molecular mechanisms underlying this association remain unclear. We recently identified 4 EAC-specific master regulator transcription factors (MRTF) ELF3, KLF5, GATA6, and EHF. In the

Conflict of interest statement

The rest of authors declare no potential conflicts of interest.

[*]**Correspondence authors:** Jian Pan, PhD, Department of Hematology and Oncology, Children's Hospital of Soochow University, Suzhou, China. Phone: +86-0512-80691508; panjian2008@163.com. De-Chen Lin, PhD, Department of Medicine, Cedars-Sinai Medical Center, 8700 Beverly Blvd, Los Angeles, CA 90048, USA. Phone: 310-423-7740. dchlin11@gmail.com.

[†]These authors contributed equally to this work.

Author Contributions

D.-C.L. conceived and devised the study. D.-C.L., S.M., B.Z., W.Y. and J.P. designed experiments and analyses. S.M., W.Y., Y.P. and B.Z. performed the experiments. Q.Y., S.M. and B.Z. performed bioinformatics and statistical analysis. J.J.B., S.J.F., L.-W.D., N.A.B. and M.R.F. contributed reagents and materials. S.M., W.Y., J.P., H.P.K. and D.-C.L. analyzed the data. H.P.K. and D.-C.L. supervised the research and wrote the manuscript.

present study, Gene Set Enrichment Analysis (GSEA) of both EAC patient samples and cell line models unbiasedly underscore fatty acid synthesis as the central pathway downstream of three MRTF (ELF3, KLF5, GATA6). Further characterizations unexpectedly identified a transcriptional feedback loop between MRTF and fatty acid synthesis, which mutually activated each other through the nuclear receptor PPARG. MRTF cooperatively promoted PPARG transcription by directly regulating its promoter and a distal EAC-specific enhancer, leading to PPARG overexpression in EAC. PPARG was also elevated in Barrett's esophagus, a recognized precursor to EAC, implying that PPARG might play a role in the intestinal metaplasia of esophageal squamous epithelium. Upregulation of PPARG increased de novo synthesis of fatty acids, phospholipids, and sphingolipids as revealed by mass spectrometry-based lipidomics. Moreover, ChIP-Seq, 4C-Seq, and a high-fat diet murine model together characterized a novel, noncanonical, and cancer-specific function of PPARG in EAC. PPARG directly regulated the ELF3 super-enhancer, subsequently activating the transcription of other MRTF through an interconnected regulatory circuitry. Together, elucidation of this novel transcriptional feedback loop of MRTF/PPARG/fatty acid synthesis advances our understanding of the mechanistic foundation for epigenomic dysregulation and metabolic alterations in EAC. More importantly, this work identifies a potential avenue for prevention and early intervention of EAC by blocking this feedback loop.

Keywords

Transcription factor; Esophageal adenocarcinoma; Fatty-acid synthesis; Gene regulation

INTRODUCTION

Esophageal cancer is classified into either squamous cell carcinoma (ESCC) or adenocarcinoma (EAC). In Western countries, while ESCC remains infrequent, the incidence of EAC has increased nearly six-fold over last three decades, representing the highest rate increase of any cancer type(1). Patients with EAC are often diagnosed at late stages and have poor quality-of-life and dismal prognosis.

In each cell type, a limited number of transcription factors (TFs) are critical for establishing cell identity by controlling gene expression programs(2). These TFs are often termed master regulator TFs (MRTFs), which occupy most cell-type-specific enhancers and super-enhancers(3). Considering that transcriptional dysregulation is a hallmark of cancer(4), characterization of MRTFs has imperative significance for the understanding of the cancer-specific transcriptome. Focusing on EAC, we recently identified 4 EAC-specific MRTFs, ELF3/KLF5/GATA6/EHF(5). These EAC-specific MRTFs form an inter-connected auto-regulatory loop by binding to each other's super-enhancers. Moreover, all 4 proteins are strongly overexpressed in EAC primary tumors compared with normal gastroesophageal junction (NGEJ) samples, and are required for EAC cell proliferation and survival(5).

Although this previous work identified a set of EAC-specific MRTFs with functional significance, important questions remain to be addressed: i) what are the key target genes and signaling pathways downstream of these MRTFs? ii) can we identify actionable targets for either prevention or treatment of EAC from such downstream target genes and signaling

pathways? To address these questions, in the present study we initially performed unbiased Gene Set Enrichment Analysis (GSEA) using both *in vivo* EAC patient samples and *in vitro* perturbation experiments, and identified fatty-acid metabolism as the most significantly enriched pathway downstream of MRTFs (Fig. 1A). This finding is of great interest, given the prominent link between fatty-acid synthesis, obesity and EAC risk. Indeed, as one of the most significant risk factors for EAC, obesity has been consistently associated with increased risk of EAC in many different cohorts(6,7).

However, the mechanisms underlying the association between obesity and EAC risk remain incompletely understood, and direct causality has not been established between obesity and EAC development. Indeed, multiple studies have suggested that obesity *per se* may not be the culprit; instead, certain dietary and/or metabolic factors in obese patients may increase the risk of EAC. Particularly, across different cohorts of patients, both high-fat diet (HFD) (8–10) and metabolic syndrome have been consistently associated with increased risk of EAC[11–14]. Supporting the importance of fatty-acid metabolism in the pathophysiology of EAC, among the metabolites from various categories (carbohydrate, amino acid, xenobiotics, lipid), fatty-acids accounted for a large faction of increased molecules in the serum of EAC patients compared with normal individuals(14). This finding is especially interesting considering that in the obese condition, adipose tissue releases more fatty-acids, which are present in both serum and nonadipose tissues(15–17). High-fat dietary similarly increases the level of lipids (including fatty-acids and triglyceride) in the serum and other tissues(18–20). Clearly, a better understanding of the molecular basis of the link between obesity, fatty-acid metabolism and EAC is of great clinical significance. Towards this end, here we explored the molecular foundation between our previously-identified MRTFs, fatty-acid metabolism and EAC, using in vivo patient samples, in vitro perturbation of cell lines, animal modeling as well as metabolomic and epigenomic profiling.

MATERIALS AND METHODS

Human cancer cell lines

Human esophageal cancer cell lines were kindly provided by the Stephen Meltzer's laboratory from Johns Hopkins University. Flo-1, SKGT4, JH-EsoAd1 and OE33 were cultured in Dulbecco's modified Eagle medium (DMEM, Gibco, USA) and TE7, KYSE30, KYSE140, KYSE150, OE19, ESO26, OACp4C and OACM5.1 were grown in RPMI-1640 medium (Gibco, USA). Both media were supplemented with 10% FBS (Omega Scientific, Tarzna, USA) and 1% penicillin-streptomycin sulfate (Thermo Scientific, USA). All cultures were maintained in a 37 °C incubator supplemented with 5% CO_2. All of the cell lines were tested for mycoplasma and verified by us using short tandem repeat analysis.

Animal experiments

Nude mice were purchased from and housed at Suzhou University. All animal studies were approved by the ethical regulations of Institutional Animal Care and Use Committee (IACUC) of Suzhou University. For the T0070907 experiment, 10 six-week-old male nude mice were subcutaneously injected with 1×10^6 ESO26 cells re-suspended in 100 μl PBS on their dorsal flanks. After 10 days, mice were separated randomly into two groups. Either

T0070907 or vehicle control (5% DMSO+45% PEG 300+H_2O) were administered twice daily by intraperitoneal injection at 5 mg/kg. Mouse weight was measured every 4 days for a total of 20 days of treatment. Mice were euthanized at the end of experiment and xenograft tumors were extracted for analyses.

In the high/low-fat diet experiments, 40 six-week-old male nude mice were fed with either high-fat chow (D12492, Researchdiets, USA) or its control low-fat chow (D12450B, controlled for calorie level) for one week, and followed by subcutaneous implantation of 1×10^6 ESO26 cells expressing either scrambled shRNA or PPARG-shRNA. Mice were maintained on either high-fat or low-fat chow for another 30 days, and tumor volumes were measured at indicated time points. At the end of experiments, mice were euthanized and xenograft tumors were dissected for further analyses.

Chromatin immunoprecipitation (ChIP)

ChIP assay was performed as described previously(5). In brief, 1×10^7 cells were harvested in 15 ml tubes and fixed with 4 ml of 1% paraformaldehyde for 10 min at room temperature, and the reaction was stopped by 2 ml of 250 mM of glycine. Samples were rinsed with 1X PBS twice and lysed with 1 ml of 1X lysis/wash buffer (150 mM NaCl, 0.5 M EDTA pH 7.5, 1M Tris pH 7.5, 0.5% NP-40). Cell pellets were resuspended in shearing buffer (1% SDS, 10 mM EDTA pH 8.0, 50 nM Tris pH 8.0) and sonicated in a Covaris sonicator. After sonication, debris were removed by centrifuge and supernatants were diluted 5X with buffer (0.01% SDS, 1% Triton X-100, 1.2 mM EDTA pH 8.0, 150 nM NaCl). Primary antibodies were added and incubated by rotation at 4°C overnight. Dynabeads Protein G beads (Life Technologies, USA) were added the next morning and incubated by rotation for additional 4 hours. Dynabeads were washed with 1X wash buffer followed by cold TE buffer. DNAs were reverse crosslinked and purified. For ChIP-Seq, DNAs were subject to library preparation and sequencing on Illumina HiSeq platform. Primer sequences for ChIP-qPCR were listed in Supplementary Table 1.

Liquid chromatography tandem mass spectrometry (LC-MS/MS)-based lipidomics

LC-MS/MS-based lipidomics was performed as described previously(21) with modifications. Briefly, the total cellular lipids were extracted with methyl tert-butyl ether (MTBE) (Sigma Aldrich) from fresh cell pellets and dried in a SpeedVac concentrator (Thermo Scientific). Lipid samples were resuspended in 50% isopropanol/50% methanol and analyzed by LC-MS/MS. Twenty microliters of lipid solution were loaded onto a 15-cm Accucore Vanquish C18 column (1.5 μm particle size, 2.1 mm diameter) and separated using an Ultimate 3000 XRS ultraperformance LC system (Thermo Scientific). The mobile phase consisted of 60% acetonitrile, 10 mM ammonium formate, 0.1% formic acid (phase A), and 90% isopropanol, 10% acetonitrile, 10 mM ammonium formate, 0.1% formic acid (phase B). The LC gradient was 35-60% B for 4 min, 60-85% B for 8 min, 85%-100% for 9 min, 100% B for 3 min, 100-35% B for 0.1 min, and 35% B for 4 min at a flow rate of 0.3 ml/min. Mass spectra were acquired by an Orbitrap Fusion Lumos Tribrid mass spectrometer (Thermo Scientific) operated in a data-dependent manner. The parameter settings for FTMS1 included orbitrap resolution (120,000), scan range (m/z 250-1,200), AGC (2×105), maximum injection time (50 ms), RF lens (50%), data type (profile), dynamic exclusion for

8s using a mass tolerance of 25 ppm, and cycle time (2 s); FTMS2 included orbitrap resolution (30,000), isolation window (1.2 m/z), activation type (HCD), collision energy (30±3%), maximum injection time (70 ms), AGC (5×104), and data type (profile). The acquired raw files were analyzed using LipidSearch (v1.4) (Thermo Scientific) for sample alignment, MS2 identification, and MS1 peak area calculation. Statistical analysis was conducted using the Perseus (v1.6.6.0) software(22), wherein the p values were calculated by two-tailed Student's t-test and corrected for multiple hypothesis testing via the Benjaminin-Hochberg method. Volcano plots were generated using the ggplot2 in the R environment (R Development Core Team; https://www.r-project.org/) (v3.5.0).

Data availability

The accession numbers for ChIP-Seq and RNA-Seq data are GEO: GSE143195.

The rest of Materials and Methods are described in Supplementary Data.

RESULTS

MRTFs (ELF3, KLF5, GATA6) functionally promote fatty-acid synthesis pathway in EAC

As introduced earlier, we recently characterized an inter-connected circuitry formed by 4 MRTFs (ELF3, KLF5, GATA6, EHF) in an EAC-specific manner(5). To explore downstream signaling pathways activated by these MRTFs in vivo, we screened unbiasedly for pathways which were positively correlated with the expression of MRTFs based on TCGA RNA-Seq data. Specifically, we first stratified EAC primary samples into MRTF-high (top 40% samples) and MRTF-low (bottom 40% samples) groups. This stratification was performed using either each individual MRTF separately or together, resulting in 5 comparisons. Next, differentially expressed genes between MRTF-high and -low groups were used to perform unbiased GSEA. Notably, the highest ranked (based on q value) hallmark pathway in MRTF-high group was fatty-acid metabolism (Fig. 1A–B). As mentioned earlier, this result was of great interest considering the strong association between obesity, fatty-acid metabolism and EAC risk.

Validating GSEA results from EAC patient samples, the fatty-acid metabolism pathway was significantly downregulated in EAC cell lines upon silencing of either ELF3, KLF5, or GATA6 (Fig. 1C). However, this pathway was not enriched in the RNA-seq of EHF-knockdown cells. Therefore, we focused on the three MRTFs (ELF3, KLF5, GATA6) for further investigations. In-depth analyses of the enriched genes in this pathway suggested that *de novo* fatty-acid synthesis was enhanced by higher MRTF expression, since multiple central enzymes for this process (ACLY, ACC, FASN, SCD, ACSS2) were all markedly decreased by knockdown of either ELF3, KLF5 or GATA6 (Fig. 1D). In contrast to most normal cells which prefer to use exogenous fatty-acids, tumor cells synthesize fatty-acids *de novo*(23,24). Indeed, heightened *de novo* fatty-acid synthesis is a metabolic feature of multiple types of cancers(24,25). We thus postulated that decreased levels of enzymes for fatty-acid synthesis upon knockdown of MRTFs might result in reduced lipid storage in EAC cells. Indeed, depletion of MRTFs decreased the total level of lipid droplets (Fig. 1E). Therefore, unbiased GSEA results from both human samples and *in vitro* knockdown

experiments demonstrate that 3 EAC-specific MRTFs (ELF3, KLF5, GATA6) functionally promote fatty-acid synthesis in EAC.

EAC MRTFs (ELF3, KLF5, GATA6) activate PPARG transcription by binding to its promoter and enhancer

To explore the mechanism(s) underlying the regulation of the three MRTFs on fatty-acid synthesis, we focused on known human master regulators of fatty-acid metabolism, including SREBFs, PPAR family, RXRs and LXRs(26–30). Following a screen of all 8 of such regulators, PPARG was identified as the only factor consistently and potently regulated by the three MRTFs at both the mRNA (Fig. 2A and Supplementary Fig. 1) and protein levels (Fig. 2B). In agreement with our recent finding(5) that these MRTFs form inter-connected circuitry, silencing each MRTF inhibited the expression of other MRTFs (Fig. 2B). We next performed rescue assays using both LipidTox staining (Fig. 2C) and qRT-PCR analyses (Fig. 2D), and over-expression of PPARG overcame the effect of KLF5-depletion, suggesting that PPARG acts as a functional mediator downstream of the three MRTFs to regulate fatty-acid metabolism.

To elucidate the regulation of MRTFs on PPARG expression, we explored the epigenomic state centering on the *PPARG* locus. Compared with nonmalignant NGEJ samples, the promoter and a distal element downstream of PPARG exhibited much higher H3K27ac signals (top 2 tracks of Fig. 2E). These two regions also showed markedly increased H3K27ac intensity in EAC relative to ESCC cell lines (3-4 tracks of Fig. 2E), indicating their potential EAC-specific activity. To explore whether this distal region functions to regulate the transcriptional activity of PPARG, we interrogated enhancer-gene linkage determined by a recent large-scale TCGA effort integrating ATAC-Seq and RNA-Seq data(31). Within 1 Mb window flanking *PPARG* locus, only two genomic regions were identified to have significantly positive correlations between ATAC-Seq peak intensity and the expression level of PPARG. Expectedly, one of the two regions was the PPARG promoter ($R = 0.958$, $P = 0.010$, Fig. 2E). Strikingly, the other one was encompassed within the distal element identified above ($R = 0.982$, $P = 0.0029$, Fig. 2E). The unbiased screen of enhancer-gene linkage identified this distal region as the only transcriptional enhancer for PPARG within 1Mb of its transcriptional start site (TSS). Further substantiating the EAC-specificity of this distal enhancer, its accessibility was noticeably high in EAC tumor samples based on ATAC-seq signals, but was completely inaccessible in either ESCC or normal esophagus squamous tissues (bottom 4 tracks of Fig. 2E). We subsequently cloned this enhancer element into luciferase reporter vector and confirmed its robust reporter activity in different EAC cells (Fig. 2F).

Importantly, our ChIP-Seq data showed that the three MRFTs (ELF3, KLF5 and GATA6) co-occupied the enhancer region, and KLF5 alone bound to PPARG promoter (5-7 tracks of Fig. 2E), suggesting that PPARG transcription is directly regulated by MRTFs in an EAC-specific manner. Indeed, luciferase reporter activity of the PPARG enhancer was significantly reduced following individual silencing of MRTFs (Fig. 2F). Moreover, PPARG was expressed significantly higher in EAC samples than either nonmalignant distal esophageal samples or ESCC samples in TCGA cohorts (Fig. 2G), consistent with our

previously finding that EAC-specific MRTFs are highly and uniquely expressed in EAC tumor samples. Indeed, the mRNA level of PPARG was the highest in EAC cells across all cancer cell lines (Supplementary Fig. 2A, data were retrieved from Cancer Cell Line Encyclopedia(32)). PPARG protein levels were validated in a panel of selected cell lines from EAC and ESCC (Supplementary Fig. 2B). These results together demonstrate that MRTF circuit (ELF3, KLF5 and GATA6) controls the transcription of PPARG by directly regulating its promoter and enhancer regions in EAC.

Since two of the three MRTFs (GATA6 and KLF5) upstream of PPARG have been reported to be upregulated in Barrett's esophagus (33,34), we next explored the expression of PPARG in this precursor state of EAC using public transcriptomic datasets (35–37). Notably, the expression of PPARG was already high in Barrett's esophagus (but not in either gastric or duodenum samples), exhibiting comparable levels with EAC samples (Supplementary Fig. 3A–C) in both datasets. In agreement with previous reports (33,34), the MRTFs showed similar expression pattern as PPARG in Barrett's esophageal samples (Supplementary Fig. 3A–C). Moreover, PPARG-targeting network exhibited consistent upregulation in Barrett's esophageal samples (but not in in either gastric or duodenum samples, Supplementary Fig. 3D–F). Together, these data show that both PPARG and its target network are already upregulated in Barrett's esophagus, indicating that PPARG might also be involved in the intestinal metaplasia of esophageal epithelial cells. In addition, the upregulation of PPARG is likely due to the high activity of its upstream master regulators (ELF3, GATA6, KLF5) in Barrett's esophageal samples.

PPARG regulates fatty-acid synthesis in EAC cells

Given the above finding that EAC-specific MRTFs promote fatty-acid synthesis through activating PPARG, we next investigated the functional contribution of PPARG to fatty-acid synthesis. PPARG knockdown potently decreased lipid droplet content in EAC cells (Fig. 3A). Moreover, unbiased pathway enrichment analysis of down-regulated genes (fold change > 0.5) from RNA-Seq data upon PPARG knockdown confirmed that lipid metabolism-related pathways ranked within the top 10 (Fig. 3B). This pathway enrichment result was reproduced by RNA-Seq of EAC cells treated with PPARG inhibitor (T0070907, Supplementary Fig. 4A). Considering the enormous structural complexity of lipid species in human cells, we next performed liquid chromatography tandem mass spectrometry (LC-MS/MS)-based lipidomic analysis(21). For robustness, three replicates for both control and knockdown samples were profiled, and high correlation between replicates was achieved (Pearson correlation coefficient ranging from 0.80-0.94, Supplementary Fig. 4B). A total of 950 lipid ions (which belonged to 24 classes of lipids) were identified and quantified (Supplementary Table 2), suggesting high sensitivity and lipidome coverage of the lipidomics methodology. This label-free quantification showed that PPARG-silencing led to the significant reduction of 173 and increased of 48 lipid species (Fig. 3C and Supplementary Fig. 5). To elucidate further how PPARG regulates fatty-acid metabolism in EAC cells, ChIP-Seq was performed with a verified ChIP-grade PPARG antibody(38) in two different EAC cell lines (OE33 and ESO26). As anticipated, top-ranked sequence motifs enriched in PPARG-binding regions were PPAR family and its canonical coactivator RXR (Fig. 3D). Canonical target genes such as *FASN* was expectedly occupied by PPARG at the

promoter region in both ESO26 and OE33 cells (Fig. 3E). Importantly, integrative analyses of RNA-Seq, ChIP-Seq and lipidomics data identified direct PPARG-downstream factors and associated lipid substrates (Fig. 3F). These target genes were enriched in *de novo* fatty-acid synthesis (ACLY, ACC, FASN and SCD), phospholipids synthesis (DGAT1, PGPS1, PEMT, CDS1, PISD) and sphingolipids synthesis (SGPL1). As a consequence, many lipid classes from these two metabolic networks (diacylglycerol (DAG), triglyceride (TAG), cytidine diphosphate diacylglycerol (CDP-DAG) and phosphatidylcholine (PC) from phospholipids; sphingomyelin (SM) and glucosylceramides (GlcCer) from sphingolipids) were decreased after PPARG depletion. Of note, some of these down-regulated lipids, such as sphingomyelin and sphingosine, are shown to have pro-survival or anti-apoptotic functions in certain cancer cells (39). Therefore, the reduction of these lipids might affect cell viability of EAC cells. We randomly selected some of the target genes for validation by qRT-PCR and Western Blotting, which confirmed the RNA-seq results (Fig. 3G and Supplementary Fig. 6). Together, these data establish a central role of PPARG in synthesis of fatty-acids, phospholipids and sphingolipids in EAC cells.

Inhibition of PPARG/fatty-acid synthesis axis potently suppresses EAC cell viability

Lipid species are major components of biological membranes, and they also have important roles for signal transduction(24,25). As a result, multiple types of tumors rely on heightened lipid synthesis for proliferation and survival(24,25). We, therefore, next investigated the biological significance of PPARG in EAC cells. Depletion of endogenous PPARG expression markedly inhibited cell proliferation (Fig. 4A) and colony growth (Fig. 4B), and increased apoptosis (Fig. 4C) across different EAC cell lines. Because PPARG was expressed higher in EAC tumors than nonmalignant distal esophageal tissues (Fig. 2G), we mimicked this *in vitro* by ectopic expression of PPARG in EAC cell lines with low endogenous levels (Fig. 4D). As a result, increased PPARG expression enhanced cell proliferation and colony formation (Fig. 4E and 4F). To further determine the functional significance of fatty-acid synthesis pathway in EAC cells, we silenced two of PPARG-downstream targets, FASN and SCD, which were key enzymes for *de novo* fatty-acid synthesis. Indeed, depletion of either FASN or SCD diminished the total level of lipid droplets (Fig. 4G and 4H) and inhibited the proliferative capacity of EAC cells (Fig. 4I).

Targeting PPARG with T0070907 inhibits EAC proliferation and survival

T0070907 is a potent and selective PPARG antagonist by covalently modifying its cysteine 313 and altering the conformation of its ligand-binding domain (40). Validating our knockdown experiments, T0070907 treatment inhibited EAC cell proliferation (Fig. 5A), colony growth (Fig. 5B) and triggered massive cell apoptosis (Fig. 5C). Confirming the on-target effect, the inhibitory function of T0070907 was dependent on the expression of PPARG, since relative to cell lines with low PPARG level, those with higher PPARG expression were significantly more sensitive to this inhibitor (Fig. 5A and 5B). Furthermore, in isogenic cell lines, PPARG knockdown (Fig. 5D) and over-expression (Fig. 5E) respectively increased and decreased IC50s of T0070907 by 6-12 fold. Consistently, T0070907 weakened the binding (Fig. 5F and Supplementary Fig. 7A) of PPARG to its target genes, such as FASN, ACC and SCD. As anticipated, the expression levels of these downstream genes were down-regulated by T0070907 (Fig. 5G and Supplementary Fig. 7B).

In a xenograft study, T0070907 dramatically inhibited the growth of EAC tumors but did not cause loss of mice weight (Fig. 5H–J). Consistent with our *in vitro* experiments, the expression of PPARG-downstream genes in the xenografts was decreased by T0070907 treatment (Fig. 5K).

PPARG cooperates with ELF3 and directly activates ELF3 super-enhancer

Following the establishment of the EAC-promoting role of PPARG through regulating fatty-acid synthesis, we next sought to explore whether PPARG harbors noncanonical, cancer-specific functions in EAC cells. To address this, we focused on the PPARG ChIP-Seq data generated in two EAC cell lines, and identified 7 shared sequence motifs among the top 20 (Fig. 6A and Supplementary Fig. 8). In addition to the consensus motifs of PPAR and RXR families, we expectedly identified TR4 (which binds to similar hormone response elements as PPARG(41)) and NUR77 (a functional cooperator of PPARG in adipocytes(42)). Surprisingly, recognition motifs of two GI-specific TFs, ELF3 and HNF4A(33,43) were highly enriched in both EAC cell lines (Fig. 6A). Other GI-specific TFs, including CDX2 and EHF, were also ranked highly, albeit not overlapped between the two cell lines (Fig. 6A). These data strongly suggest that PPARG-occupancy in EAC genome exhibits EAC-specific features, with possible co-occupancy with EAC-specific TFs. Among these, ELF3 was particularly interesting, since it is one of the key EAC-specific MRTFs we previously identified(5), which also controls PPARG transcription (Figs. 1–2). Importantly, validating the motif enrichment analysis, ChIP-Seq of ELF3 revealed a total of 838 co-binding peaks with PPARG (Fig. 6B), which was highly significant (Supplementary Fig. 9). Indeed, binding peaks of the two TFs strongly aligned (Fig. 6C). Prominent H3K27Ac signals flanked the regions co-occupied by these two TFs, suggesting that PPARG/ELF3 co-binding is associated with active transcription. Notably, compared with PPARG solo-binding regions, these co-binding regions were significantly more enriched in super-enhancers (13.4% vs 8.1%, P value = 1.6e-14, Fig. 6D), congruent with our previous finding that MRTFs favor binding to super-enhancers over typical-enhancers(5,44,45). Super-enhancers of several known tumor-promoting genes, such as CDX2, FOSL2, MCL1 and HES1, were all highly ranked in PPARG/ELF3 co-binding regions (Fig. 6D and Supplementary Table 3), indicating that PPARG/ELF3 may co-regulate the expression of key cancer genes in EAC.

One of the most important characteristics of EAC-specific MRTFs is their unique capability of forming an inter-connected regulatory circuitry by binding to each other's super-enhancers(5), a transcriptional paradigm also observed in other cell types(3,45–47). Given the prominent co-binding of PPARG/ELF3 across super-enhancers, we speculated that PPARG might similarly participate in the inter-connected regulatory circuitry of MRTFs. Notably, among their 838 co-binding regions, a super-enhancer assigned to ELF3 itself was ranked as No. 4 in terms of the H3K27ac intensity (Fig. 6D). By integrating 4C-Seq, CRISPR interference (CRISPRi) and luciferase reporter assay, we recently identified and confirmed five functional constituent enhancers (E1-E5) within this ELF3 super-enhancer(5). Notably, all but E5 element exhibited much stronger H3K27ac intensity in EAC tumors compared with NGEJ samples (Supplementary Fig. 10). Consistently, these enhancers showed higher chromatin accessibility in EAC samples than either ESCC or normal esophageal squamous samples (Supplementary Fig. 10).

Importantly, our ChIP-Seq data showed that PPARG interacted with these constituent enhancers (Fig. 6E). Luciferase reporter assay was performed and showed that the activities of three of the enhancers (E1, E2, E4) were reduced after PPARG inhibition (Fig. 6E and 6F). ChIP-qPCR confirmed that PPARG occupied E1, E2 and E4 regions (Supplementary Fig. 11). Moreover, both mRNA (Fig. 6G) and protein levels of ELF3 (Fig. 6H) were significantly decreased following PPARG silencing, confirming that PPARG directly regulates the transcription of ELF3 by interacting with its super-enhancer. The levels of other MRTFs were also downregulated by PPARG knockdown, consistent with the model of inter-connected co-regulatory circuitry (Fig. 6G and 6H). Together, these results reveal that PPARG cooperates with ELF3 in binding to hundreds of typical- and super-enhancers in EAC cells, and one of such top-ranked super-enhancers is associated with ELF3 itself. By activating this ELF3 super-enhancer, PPARG directly promotes ELF3 transcription, thereby further regulating the transcription of other MRTFs through an inter-connected co-regulatory circuitry (Fig. 6I).

Identification of a transcriptional feedback loop of Fatty-acid/PPARG/MRTF in EAC

To explore further the above reciprocal regulation between PPARG and MRTFs through activating each other's EAC-specific enhancers (Fig. 2 and Fig. 6), we treated EAC cells *in vitro* with three different free fatty-acids: stearic acid (saturated, C18:0), oleic acid (monounsaturated, C18:1) and arachidonic acid (AA, polyunsaturated, C20:4) which are known natural ligands to activate PPARG(48,49). Importantly, supplement of free fatty-acids induced the expression of MRTFs across different EAC cells (Fig. 7A). Moreover, this induction was dependent on the activity of PPARG, since the effect was abolished in PPARG-knockdown cells (Fig. 7A). Luciferase reporter assay confirmed that PPARG-regulated enhancers were activated by free fatty-acids (Fig. 7B, Supplementary Fig. 12). Together, these data not only substantiate our earlier findings that PPARG promotes the transcription of EAC-specific MRTFs, but also identify a "transcriptional feedback loop" between fatty-acid/PPARG/MRTF (Fig. 7C). Given the strong clinical association between obesity, high-fat diet (HFD) and EAC, this feedback loop is of great interest. Specifically, in obese individuals, adipose tissue is more hypertrophic and has a higher basal rate of fatty-acid release(15–17). Increased fatty-acid levels are present in both the serum and non-adipose tissues(15–17), a systematic metabolic effect similarly induced by HFD(18). Therefore, in gastroesophageal junction tissues, obesity and/or HFD may elevate PPARG activity, thereby activating this transcriptional feedback loop. Because of key oncogenic functions of MRTFs in EAC, this feedback loop may thus promote EAC viability in the obese/HFD condition (Fig. 7C).

We further tested this feedback loop *in vivo* by investigating transplanted tumors in an HFD murine model. A lard-based HFD was selected because it has been confirmed to increase the levels of free fatty-acids in rodents (19,20,50) . Notably, compared with the low-fat diet (LFD) group, EAC xenograft tumors developed faster and larger in the HFD group (Fig. 7D–F). Importantly, the growth of xenograft tumors was potently inhibited upon loss of PPARG regardless of the diet conditions (Fig. 7D–F), strongly suggesting that high-fat chow promotes EAC growth *in vivo* through activating PPARG. Moreover, in xenograft samples, the expression levels of both MRTFs and canonical PPARG-target genes were upregulated

by high-fat chow, which was reversed by PPARG knockdown (Fig. 7G). Taken together, these results corroborate the presence of a transcriptional feedback loop of fatty-acid/PPARG/MRTF which promote the growth of EAC tumors *in vivo*.

DISCUSSION

The present work was aimed to identify key target genes and signaling pathways downstream of EAC-specific MRTFs which may contain actionable targets for prevention, intervention or treatment of this deadly GI cancer. Toward this goal, four different sets of data highlight the link between the three MRFTs (ELF3, KLF5 and GATA6) and fatty-acid metabolism in EAC biology: i) From unbiased GSEA analyses from EAC patients, fatty-acid metabolism is the most significantly enriched pathway in MRTF-high samples (Fig. 1A); ii) Fatty-acid metabolism pathway is strongly downregulated upon MRTF knockdown *in vitro* (Fig. 1C and 1D); iii) MRTFs promote the expression of multiple key enzymes for fatty-acid synthesis and regulate the abundance of lipid droplets (Fig. 1E and 1F); iv) Levels of various fatty-acid metabolites are increased in EAC patients(14). Specifically, among a total of 64 pan-metabolites (involving amino acids, carbohydrates, lipids, xenobiotics) that differed significantly between EAC cases and controls, it is striking that almost half (29/64) are fatty-acids, including oleate and stearate which were used in this work (Fig. 7A–B). Moreover, these fatty-acids are increased significantly in two independent EAC cohorts (a total of 120 individuals)(14). These data reinforce that fatty-acid synthesis indeed accounts significantly for altered metabolic programs in EAC, validating our unbiased GSEA results from patient samples (Fig. 1A). Therefore, bioinformatical, biological and epidemiological data together underscore MRTF/fatty-acid synthesis as a key pathway in EAC pathophysiology.

In searching for the mechanisms underlying MRTF/fatty-acid synthesis in EAC, we identified PPARG as a central mediator for this cascade. MRTFs promote PPARG transcription through direct activation of PPARG promoter and an EAC-specific enhancer. Indeed, PPARG level is higher in EAC tumors than nonmalignant distal esophageal tissues. Moreover, cancer-specific activity of EAC MRTFs conceivably explains the specific expression pattern of PPARG across all tumor types (Supplementary Fig. 2A). Interestingly, PPARG and its target network are upregulated in Barrett's esophagus (Supplementary Fig. 3). Nevertheless, this result is not unexpected since two of the three master regulators upstream of PPARG (GATA6 and KLF5) have already been reported to be upregulated in Barrett's esophagus samples (51,52). Indeed, we verified that all three MRTFs were comparably high in Barrett's esophagus v.s. EAC samples. These results imply that PPARG might contribute to the metaplasia of esophageal squamous cells and not just the progression of EAC, which requires future functional characterization.

PPARG plays an essential role in adipocyte differentiation, and acts as a key regulator of lipid metabolism in adipocytes(53). However, in the context of cancer biology, PPARG appears to have complex and opposite functions. For example, in bladder, liver and prostate cancers, over-expression of PPARG promotes the proliferation and survival of tumor cells(54–56). In contrast, PPARG plays an anti-proliferative role in several types of cancers, such as breast(57) and lung(58) cancers. Therefore, the functional role of PPARG in tumor appears to be highly context-dependent. Here, our *in vitro* and *in vivo* data confirm that

PPARG contributes to the proliferation and viability of EAC cells. More importantly, the current data elucidate two major mechanisms underlying the pro-tumor property of PPARG in EAC: i) the canonical, general function in regulating fatty-acid metabolism, and ii) the noncanonical, EAC-specific function in promoting the transcription of ELF3.

With respect to the canonical function of PPARG, both lipid droplet staining and RNA-Seq data confirm the essential role of PPARG in fatty-acid metabolism in EAC cells. Further integrative analyses of ChIP-Seq and lipidomics data unbiasedly identify many direct PPARG-target genes and associated lipid substrates. The perturbation of lipidome (affecting ~120 lipid species) caused by PPARG-inhibition likely reduces the fitness of EAC cells. Indeed, knockdown of either FASN or SCD, primary enzymes for de novo fatty-acids synthesis, similarly suppresses EAC cell proliferation, substantiating that EAC cells rely on a hyperactive fatty-acid synthesis pathway. Mechanistically, the addiction of EAC cells to fatty-acid production may be because lipids are not only components of biological membranes, but have important roles for signal transductions (e.g., acylation of WNT and palmitoylation of RAS)(25).

Compared with the canonical role, the EAC-specific and noncanonical function of PPARG is even more intriguing. In addition to the classic PPAR motif, we quite unexpectedly discovered sequence motifs of GI-specific TFs (ELF3, HNF4A, EHF, CDX2) enriched in PPARG-binding peaks in EAC cell lines. In particular, ELF3 and EHF are EAC-specific MRTFs, suggesting that PPARG may cooperate with MRTFs in the occupancy of the EAC genome. Indeed, ChIP-Seq data confirm that ELF3 and PPARG co-occupy over 800 H3K27ac+ genomic regions. In addition, their co-binding regions are significantly more enriched in super-enhancers than typical-enhancers, in agreement with the finding that MRTFs favor regulating super-enhancers. Moreover, one top-ranked super-enhancer co-bound by ELF3/PPARG is assigned to ELF3 itself. Because of the unique capabilities of MRTFs in co-regulation of each other's super-enhancers through an inter-connected circuitry(5), we postulated that PPARG might also engage such co-regulatory circuitry given its co-occupancy on ELF3 super-enhancer. Indeed, 4C-Seq, luciferase reporter assay and qRT-PCR analyses together reveal that PPARG directly regulates ELF3 super-enhancer and, as a consequence, activates the transcription of other MRTFs through the inter-connected co-regulatory circuitry.

Identification of this noncanonical function of PPARG in regulating MRTF expression has both scientific and clinical significance. In particular, as functional PPARG agonists, the levels of fatty-acids are significantly higher in obesity(15–17) or HFD conditions(18–20) in both serum and nonadipose tissues. Moreover, as mentioned earlier, increased levels of fatty-acids are found in the serum of EAC patients(14). Combining these previously-established findings with our current data indicates the possible presence of a transcriptional feedback loop of fatty-acid/PPARG/MRTF in EAC cells. Indeed, two sets of data support the existence of such a feedback loop: i) supplementation of free fatty-acids *in vitro*; ii) high-fat diet murine model. Therefore, obesity or HFD may elevate PPARG activity in gastroesophageal cells, thereby activating the transcriptional feedback loop which increases the expression of MRTFs. Because of the oncogenic property of EAC-specific MRTFs, this feedback loop may promote EAC growth (Fig. 7C). However, one should keep in mind that

this feedback model does not rule out other possible mechanisms underlying obesity/HFD and EAC, given that obesity, HFD and high BMI induce systematic, whole-body inflammation. For example, a recent study showed that HFD could significantly change the esophageal microenvironment and gut microbiome, induce inflammation and accelerate EAC development(13). Therefore, multiple different pathogenic factors induced by obesity/HFD possibly coordinate to promote the development and/or progression of EAC.

In conclusion, this study identifies fatty-acid synthesis as the key downstream pathway of EAC-specific MRTFs. We establish both canonical and noncanonical functions of PPARG in EAC cells and elucidate a novel transcriptional feedback loop, wherein MRTFs and PPARG reciprocally activate each other's EAC-specific enhancers. The characterization of this transcriptional loop may help the development of novel strategies for EAC prevention and early intervention. For example, targeting fatty-acid synthesis pathway in obese/HFD individuals with high-risk of EAC (e.g., those with refractory or high-grade Barrett's esophagus) may offer potential benefit to reduce the risk of EAC development. Moreover, inhibition of PPARG activity (e.g., by PPARG antagonists) to block this feedback loop may also warrant further preclinical and clinical investigations for this cancer.

Supplementary Material

Refer to Web version on PubMed Central for supplementary material.

ACKNOWLEDGEMENTS

D-C.L is supported by the DeGregorio Family Foundation, the Price Family Foundation as well as Samuel Oschin Comprehensive Cancer Institute (SOCCI) at Cedars-Sinai Medical Center through the Translational Pipeline Discovery Fund. This work was supported by NIH/NCI under award (R37CA237022) to D.-C.L. This research is also partially supported by the National Research Foundation Singapore under its Singapore Translational Research (STaR) Investigator Award (NMRC/STaR/0021/2014) and administered by the Singapore Ministry of Health's National Medical Research Council (NMRC), the NMRC Centre Grant awarded to National University Cancer Institute of Singapore, the National Research Foundation Singapore and the Singapore Ministry of Education under its Research Centres of Excellence initiatives (to H.P.K).

References

1. Edgren G, Adami HO, Weiderpass E, Nyren O. A global assessment of the oesophageal adenocarcinoma epidemic. Gut 2013;62:1406–14 [PubMed: 22917659]
2. Whyte WA, Orlando DA, Hnisz D, Abraham BJ, Lin CY, Kagey MH, et al. Master transcription factors and mediator establish super-enhancers at key cell identity genes. Cell 2013;153:307–19 [PubMed: 23582322]
3. Boyer LA, Lee TI, Cole MF, Johnstone SE, Levine SS, Zucker JP, et al. Core transcriptional regulatory circuitry in human embryonic stem cells. Cell 2005;122:947–56 [PubMed: 16153702]
4. Bradner JE, Hnisz D, Young RA. Transcriptional Addiction in Cancer. Cell 2017;168:629–43 [PubMed: 28187285]
5. Chen L, Huang M, Plummer J, Pan J, Jiang YY, Yang Q, et al. Master transcription factors form interconnected circuitry and orchestrate transcriptional networks in oesophageal adenocarcinoma. Gut 2020;69:630–40 [PubMed: 31409603]
6. Turati F, Tramacere I, La Vecchia C, Negri E. A meta-analysis of body mass index and esophageal and gastric cardia adenocarcinoma. Ann Oncol 2013;24:609–17 [PubMed: 22898040]
7. Whiteman DC, Sadeghi S, Pandeya N, Smithers BM, Gotley DC, Bain CJ, et al. Combined effects of obesity, acid reflux and smoking on the risk of adenocarcinomas of the oesophagus. Gut 2008;57:173–80 [PubMed: 17932103]

8. O'Doherty MG, Cantwell MM, Murray LJ, Anderson LA, Abnet CC. Dietary fat and meat intakes and risk of reflux esophagitis, Barrett's esophagus and esophageal adenocarcinoma. International journal of cancer 2011;129:1493–502 [PubMed: 21455992]
9. Lagergren K, Lindam A, Lagergren J. Dietary proportions of carbohydrates, fat, and protein and risk of oesophageal cancer by histological type. PloS one 2013;8:e54913 [PubMed: 23349988]
10. He D, Huang X, Wang Z-P, Chen D, Chen J, Duan C-Y. Dietary fat intake and risk of esophageal carcinoma: a meta-analysis of observational studies. Oncotarget 2017;8:99049–56 [PubMed: 29228750]
11. Drahos J, Li L, Jick SS, Cook MB. Metabolic syndrome in relation to Barrett's esophagus and esophageal adenocarcinoma: Results from a large population-based case-control study in the Clinical Practice Research Datalink. Cancer Epidemiol 2016;42:9–14 [PubMed: 26972225]
12. Drahos J, Ricker W, Pfeiffer RM, Cook MB. Metabolic syndrome and risk of esophageal adenocarcinoma in elderly patients in the United States: An analysis of SEER-Medicare data. Cancer 2017;123:657–65 [PubMed: 27861759]
13. Münch NS, Fang HY, Ingermann J, Maurer HC, Anand A, Kellner V, et al. High-Fat Diet Accelerates Carcinogenesis in a Mouse Model of Barrett's Esophagus via Interleukin 8 and Alterations to the Gut Microbiome. Gastroenterology 2019;157:492–506.e2 [PubMed: 30998992]
14. Sanchez-Espiridion B, Liang D, Ajani JA, Liang S, Ye Y, Hildebrandt MA, et al. Identification of Serum Markers of Esophageal Adenocarcinoma by Global and Targeted Metabolic Profiling. Clin Gastroenterol Hepatol 2015;13:1730–7.e9 [PubMed: 25998788]
15. Opie LH, Walfish PG. Plasma free fatty acid concentrations in obesity. N Engl J Med 1963;268:757–60 [PubMed: 13940209]
16. Björntorp P, Bergman H, Varnauskas E. Plasma free fatty acid turnover rate in obesity. Acta Med Scand 1969;185:351–6 [PubMed: 5806343]
17. Arner P, Rydén M. Fatty Acids, Obesity and Insulin Resistance. Obes Facts 2015;8:147–55 [PubMed: 25895754]
18. Raatz SK, Bibus D, Thomas W, Kris-Etherton P. Total fat intake modifies plasma fatty acid composition in humans. J Nutr 2001;131:231–4 [PubMed: 11160538]
19. Liu T-W, Heden TD, Matthew Morris E, Fritsche KL, Vieira-Potter VJ, Thyfault JP. High-Fat Diet Alters Serum Fatty Acid Profiles in Obesity Prone Rats: Implications for In Vitro Studies. Lipids 2015;50
20. Wang X-H, Li C-Y, Muhammad I, Zhang X-Y. Fatty acid composition in serum correlates with that in the liver and non-alcoholic fatty liver disease activity scores in mice fed a high-fat diet. Environ Toxicol Pharmacol 2016;44:140–50 [PubMed: 27179602]
21. Breitkopf SB, Ricoult SJH, Yuan M, Xu Y, Peake DA, Manning BD, et al. A relative quantitative positive/negative ion switching method for untargeted lipidomics via high resolution LC-MS/MS from any biological source. Metabolomics 2017;13 [PubMed: 29249917]
22. Tyanova S, Temu T, Sinitcyn P, Carlson A, Hein MY, Geiger T, et al. The Perseus computational platform for comprehensive analysis of (prote)omics data. Nat Methods 2016;13:731–40 [PubMed: 27348712]
23. Medes G, Thomas A, Weinhouse S. Metabolism of neoplastic tissue. IV. A study of lipid synthesis in neoplastic tissue slices in vitro. Cancer Res 1953;13:27–9 [PubMed: 13032945]
24. Currie E, Schulze A, Zechner R, Walther TC, Farese RV. Cellular fatty acid metabolism and cancer. Cell Metab 2013;18:153–61 [PubMed: 23791484]
25. Röhrig F, Schulze A. The multifaceted roles of fatty acid synthesis in cancer. Nat Rev Cancer 2016;16:732–49 [PubMed: 27658529]
26. Shimano H, Sato R. SREBP-regulated lipid metabolism: convergent physiology - divergent pathophysiology. Nature reviews Endocrinology 2017;13:710–30
27. Varga T, Czimmerer Z, Nagy L. PPARs are a unique set of fatty acid regulated transcription factors controlling both lipid metabolism and inflammation. Biochim Biophys Acta 2011;1812:1007–22 [PubMed: 21382489]
28. Keller H, Dreyer C, Medin J, Mahfoudi A, Ozato K, Wahli W. Fatty acids and retinoids control lipid metabolism through activation of peroxisome proliferator-activated receptor-retinoid X

receptor heterodimers. Proceedings of the National Academy of Sciences of the United States of America 1993;90:2160–4 [PubMed: 8384714]

29. Hong C, Tontonoz P. Liver X receptors in lipid metabolism: opportunities for drug discovery. Nature reviews Drug discovery 2014;13:433–44 [PubMed: 24833295]
30. Jump DB, Tripathy S, Depner CM. Fatty acid-regulated transcription factors in the liver. Annu Rev Nutr 2013;33:249–69 [PubMed: 23528177]
31. Corces MR, Granja JM, Shams S, Louie BH, Seoane JA, Zhou W, et al. The chromatin accessibility landscape of primary human cancers. Science (New York, NY) 2018;362
32. Ghandi M, Huang FW, Jané-Valbuena J, Kryukov GV, Lo CC, McDonald ER, et al. Next-generation characterization of the Cancer Cell Line Encyclopedia. Nature 2019;569:503–8 [PubMed: 31068700]
33. Rogerson C, Britton E, Withey S, Hanley N, Ang YS, Sharrocks AD. Identification of a primitive intestinal transcription factor network shared between esophageal adenocarcinoma and its precancerous precursor state. Genome Res 2019;29:723–36 [PubMed: 30962179]
34. Rogerson C, Ogden S, Britton E, Ang Y, Sharrocks AD. Repurposing of KLF5 activates a cell cycle signature during the progression from Barrett's Oesophagus to Oesophageal Adenocarcinoma. bioRxiv 2020:2020.02.10.941872
35. Maag JLV, Fisher OM, Levert-Mignon A, Kaczorowski DC, Thomas ML, Hussey DJ, et al. Novel Aberrations Uncovered in Barrett's Esophagus and Esophageal Adenocarcinoma Using Whole Transcriptome Sequencing. Molecular cancer research : MCR 2017;15:1558–69 [PubMed: 28751461]
36. Kimchi ET, Posner MC, Park JO, Darga TE, Kocherginsky M, Karrison T, et al. Progression of Barrett's metaplasia to adenocarcinoma is associated with the suppression of the transcriptional programs of epidermal differentiation. Cancer research 2005;65:3146–54 [PubMed: 15833844]
37. Owen RP, White MJ, Severson DT, Braden B, Bailey A, Goldin R, et al. Single cell RNA-seq reveals profound transcriptional similarity between Barrett's oesophagus and oesophageal submucosal glands. Nature communications 2018;9:4261
38. Sim CK, Kim SY, Brunmeir R, Zhang Q, Li H, Dharmasegaran D, et al. Regulation of white and brown adipocyte differentiation by RhoGAP DLC1. PloS one 2017;12:e0174761 [PubMed: 28358928]
39. Ogretmen B Sphingolipid metabolism in cancer signalling and therapy. Nature reviews Cancer 2018;18:33–50 [PubMed: 29147025]
40. Lee G, Elwood F, McNally J, Weiszmann J, Lindstrom M, Amaral K, et al. T0070907, a selective ligand for peroxisome proliferator-activated receptor gamma, functions as an antagonist of biochemical and cellular activities. J Biol Chem 2002;277:19649–57 [PubMed: 11877444]
41. Lin SJ, Yang DR, Yang G, Lin CY, Chang HC, Li G, et al. TR2 and TR4 Orphan Nuclear Receptors: An Overview. Curr Top Dev Biol 2017;125:357–73 [PubMed: 28527578]
42. Duszka K, Bogner-Strauss JG, Hackl H, Rieder D, Neuhold C, Prokesch A, et al. Nr4a1 is required for fasting-induced down-regulation of Pparγ2 in white adipose tissue. Mol Endocrinol 2013;27:135–49 [PubMed: 23250487]
43. Pan J, Silva TC, Gull N, Yang Q, Plummer J, Chen S, et al. Lineage-Specific Epigenomic and Genomic Activation of the Oncogene HNF4A Promotes Gastrointestinal Adenocarcinomas. bioRxiv 2019:812149
44. Jiang Y, Jiang YY, Xie JJ, Mayakonda A, Hazawa M, Chen L, et al. Co-activation of super-enhancer-driven CCAT1 by TP63 and SOX2 promotes squamous cancer progression. Nature communications 2018;9:3619
45. Jiang Y-Y, Jiang Y, Li C-Q, Zhang Y, Dakle P, Kaur H, et al. TP63, SOX2 and KLF5 Establish Core Regulatory Circuitry and Construct Cancer Specific Epigenome in Esophageal Squamous Cell Carcinoma. bioRxiv 2019:825372
46. Odom DT, Zizlsperger N, Gordon DB, Bell GW, Rinaldi NJ, Murray HL, et al. Control of pancreas and liver gene expression by HNF transcription factors. Science (New York, NY) 2004;303:1378–81
47. Lin CY, Erkek S, Tong Y, Yin L, Federation AJ, Zapatka M, et al. Active medulloblastoma enhancers reveal subgroup-specific cellular origins. Nature 2016;530:57–62 [PubMed: 26814967]

48. Kliewer SA, Sundseth SS, Jones SA, Brown PJ, Wisely GB, Koble CS, et al. Fatty acids and eicosanoids regulate gene expression through direct interactions with peroxisome proliferator-activated receptors alpha and gamma. Proceedings of the National Academy of Sciences of the United States of America 1997;94:4318–23 [PubMed: 9113987]

49. Marion-Letellier R, Savoye G, Ghosh S. Fatty acids, eicosanoids and PPAR gamma. Eur J Pharmacol 2016;785:44–9 [PubMed: 26632493]

50. Buettner R, Parhofer KG, Woenckhaus M, Wrede CE, Kunz-Schughart LA, Schölmerich J, et al. Defining high-fat-diet rat models: metabolic and molecular effects of different fat types. J Mol Endocrinol 2006;36:485–501 [PubMed: 16720718]

51. Rogerson C, Britton E, Withey S, Hanley N, Ang YS, Sharrocks AD. Identification of a primitive intestinal transcription factor network shared between esophageal adenocarcinoma and its precancerous precursor state. Genome research 2019;29:723–36 [PubMed: 30962179]

52. Rogerson C, Ogden S, Britton E, Ang Y, Sharrocks AD. Repurposing of KLF5 activates a cell cycle signature during the progression from a precursor state to oesophageal adenocarcinoma. eLife 2020;9

53. Lehrke M, Lazar MA. The many faces of PPARgamma. Cell 2005;123:993–9 [PubMed: 16360030]

54. Goldstein JT, Berger AC, Shih J, Duke FF, Furst L, Kwiatkowski DJ, et al. Genomic Activation of Reveals a Candidate Therapeutic Axis in Bladder Cancer. Cancer Res 2017;77:6987–98 [PubMed: 28923856]

55. Patitucci C, Couchy G, Bagattin A, Caneque T, de Reynies A, Scoazec JY, et al. Hepatocyte nuclear factor 1alpha suppresses steatosis-associated liver cancer by inhibiting PPARgamma transcription. The Journal of clinical investigation 2017;127:1873–88 [PubMed: 28394260]

56. Ahmad I, Mui E, Galbraith L, Patel R, Tan EH, Salji M, et al. Sleeping Beauty screen reveals Pparg activation in metastatic prostate cancer. Proc Natl Acad Sci U S A 2016;113:8290–5 [PubMed: 27357679]

57. Bonofiglio D, Cione E, Qi H, Pingitore A, Perri M, Catalano S, et al. Combined low doses of PPARgamma and RXR ligands trigger an intrinsic apoptotic pathway in human breast cancer cells. Am J Pathol 2009;175:1270–80 [PubMed: 19644018]

58. Bren-Mattison Y, Van Putten V, Chan D, Winn R, Geraci MW, Nemenoff RA. Peroxisome proliferator-activated receptor-gamma (PPAR(gamma)) inhibits tumorigenesis by reversing the undifferentiated phenotype of metastatic non-small-cell lung cancer cells (NSCLC). Oncogene 2005;24:1412–22 [PubMed: 15608671]

Significance Statement

Findings elucidate a transcriptional feedback loop linking epigenomic dysregulation and metabolic alterations in EAC, indicating that blocking this feedback loop could be a potential therapeutic strategy in high-risk individuals.

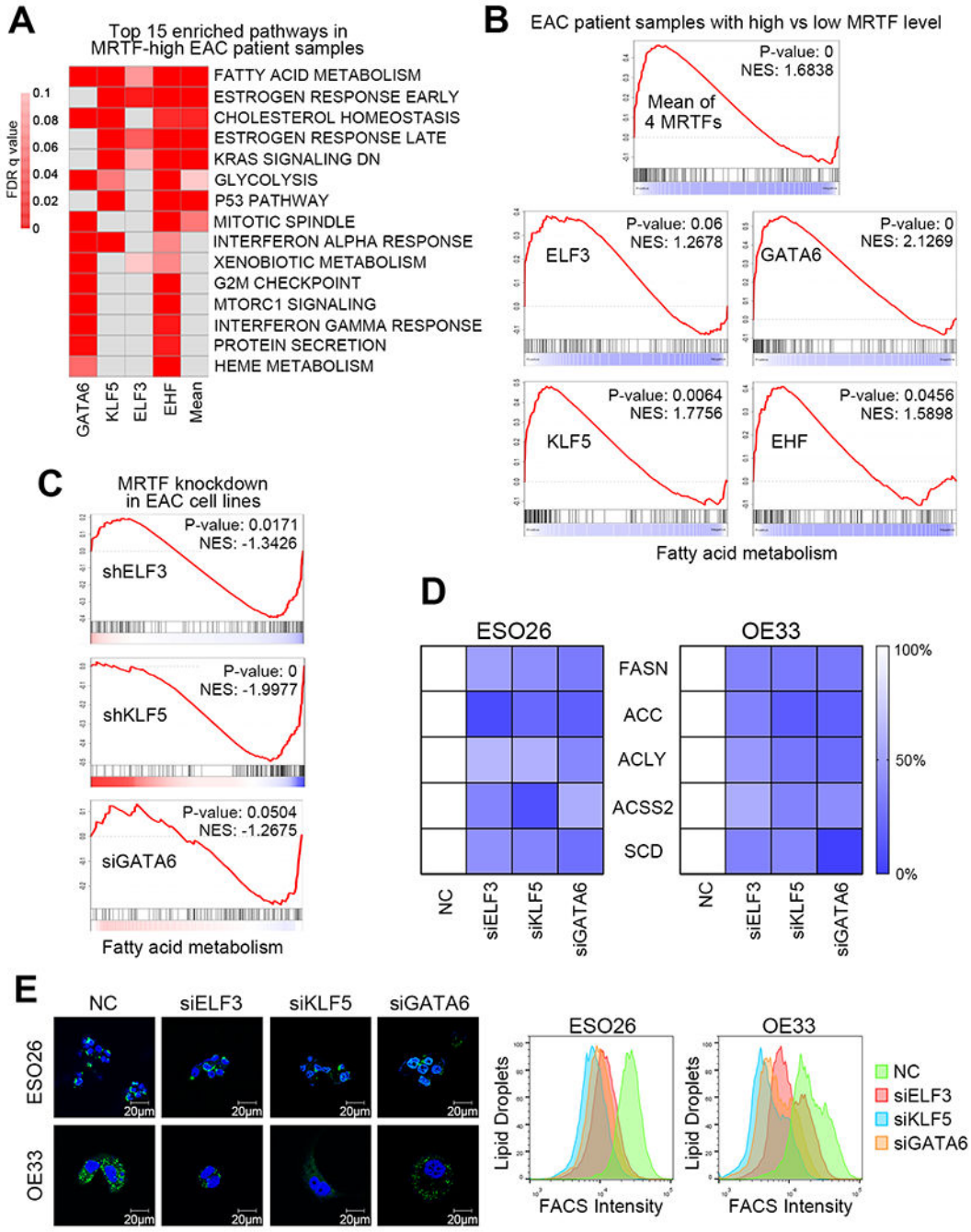

Figure 1. EAC-specific MRTFs promote fatty-acid synthesis pathway

(A) Heatmap of GSEA results of top 15 enriched hallmark pathways in MRTF-high expression (top 40%) vs MRTF-low expression (bottom 40%) EAC samples from TCGA. The average level of the 4 MRTFs was used as the "Mean" group. (B) Individual GSEA plots of fatty-acid metabolism pathway as in panel (A). (C) GSEA plots of RNA-seq upon silencing of either ELF3 or KLF5 in ESO26 cells, and silencing of GATA6 in OE19 cells. The RNA-Seq data of knockdown of ELF3 or KLF5 were generated by our group, while the data of GATA6 knockdown was conducted by Rogerson *et al* (33). (D) Heatmap of fold

changes of mRNA levels of key enzymes for *de novo* fatty-acids synthesis following siRNA knockdown of either ELF3, KLF5 or GATA6 in ESO26 and OE33 cells. (E) Confocal images (left panel) and flow cytometry analyses (right panel) of lipid droplet in the presence and absence of either ELF3, KLF5 or GATA6 knockdown in ESO26 and OE33 cells.

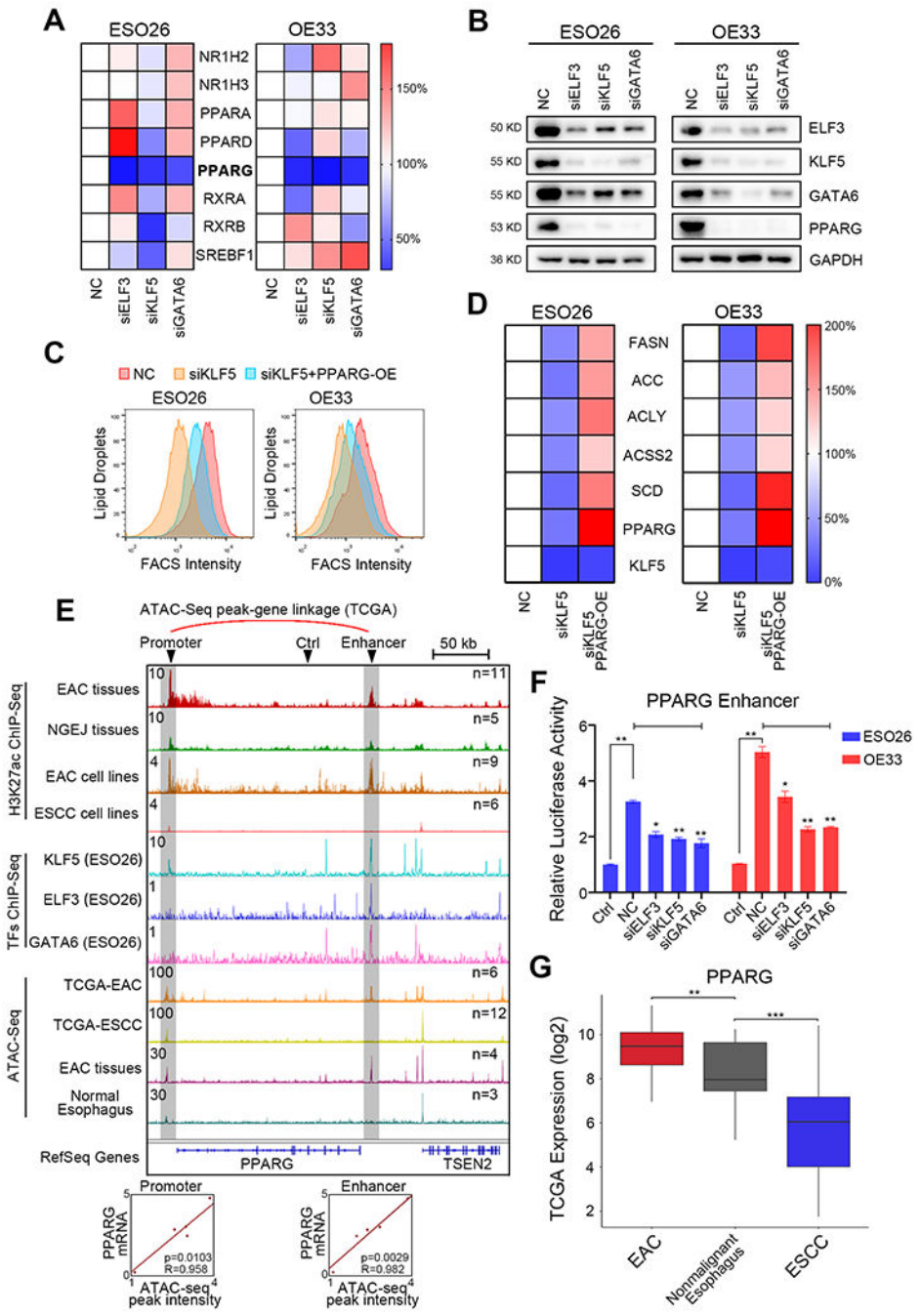

Figure 2. MRTFs directly activate both the promoter and enhancer of PPARG in an EAC-specific manner

(A) Changes in mRNA expression of eight regulators of fatty-acid metabolism upon knockdown of MRTFs. (B) Western blot validating the change of PPARG. (C) Flow cytometry analyses of lipid droplet and (D) mRNA levels of central enzymes for *de novo* fatty-acid synthesis after either KLF5 knockdown alone or combined with PPARG over-expression. (E) IGV line plots of the H3K27Ac ChIP-Seq, MRTF ChIP-Seq and ATAC-Seq in indicated samples. Signal values of normalized peak intensity are shown on the upper left corner. Number of samples for each track is shown on the upper right corner. Scatter plots at

the bottom show the correlation between ATAC-Seq peaks and PPARG mRNA expression. Each dot is a TCGA EAC sample. All ChIP-seq data were generated internally; ATAC-Seq were from either TCGA or Rogerson *et al* (bottom 2 tracks)(33). (F) Luciferase reporter assays in ESO26 and OE33 cells. PPARG enhancer and a negative control (Ctrl) region were separately cloned into luciferase reporter vector. Mean±SD are shown, n=3. *, $p<0.05$; **, $p<0.01$. (G) mRNA expression of PPARG in esophageal cancer and nonmalignant distal esophageal tissues from TCGA.

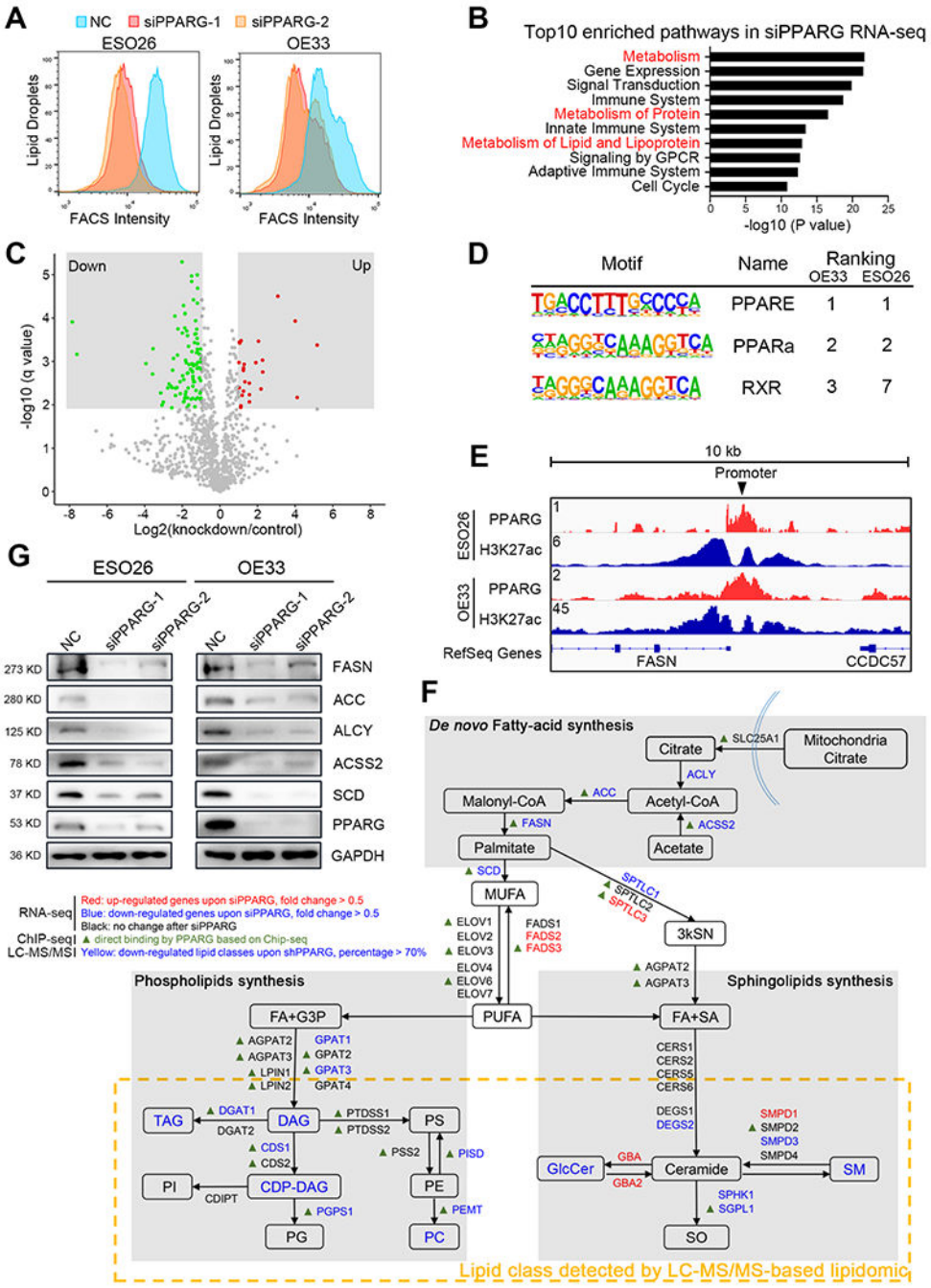

Figure 3. PPARG regulates fatty-acid synthesis in EAC cells

(A) Flow cytometry analyses of lipid droplet in the presence and absence of PPARG knockdown. (B) Top 10 enriched pathways of down-regulated genes upon PPARG knockdown in ESO26 cells. (C) Volcano plot of LC-MS/MS-based lipidomics after PPARG knockdown. Each dot is one lipid species. (D) Top ranked TF-binding motifs in PPARG ChIP-Seq in both ESO26 and OE33 cells. (E) IGV plots of H3K27Ac and PPARG ChIP-Seq at the *FASN* loci in ESO26 and OE33 cells. (F) Schematic diagram showing the regulation of lipid synthesis pathways by PPARG via integration of RNA-Seq, ChIP-Seq and

lipidomics data. (G) Western blotting of the key enzymes for *de novo* synthesis of fatty-acids following PPARG-knockdown.

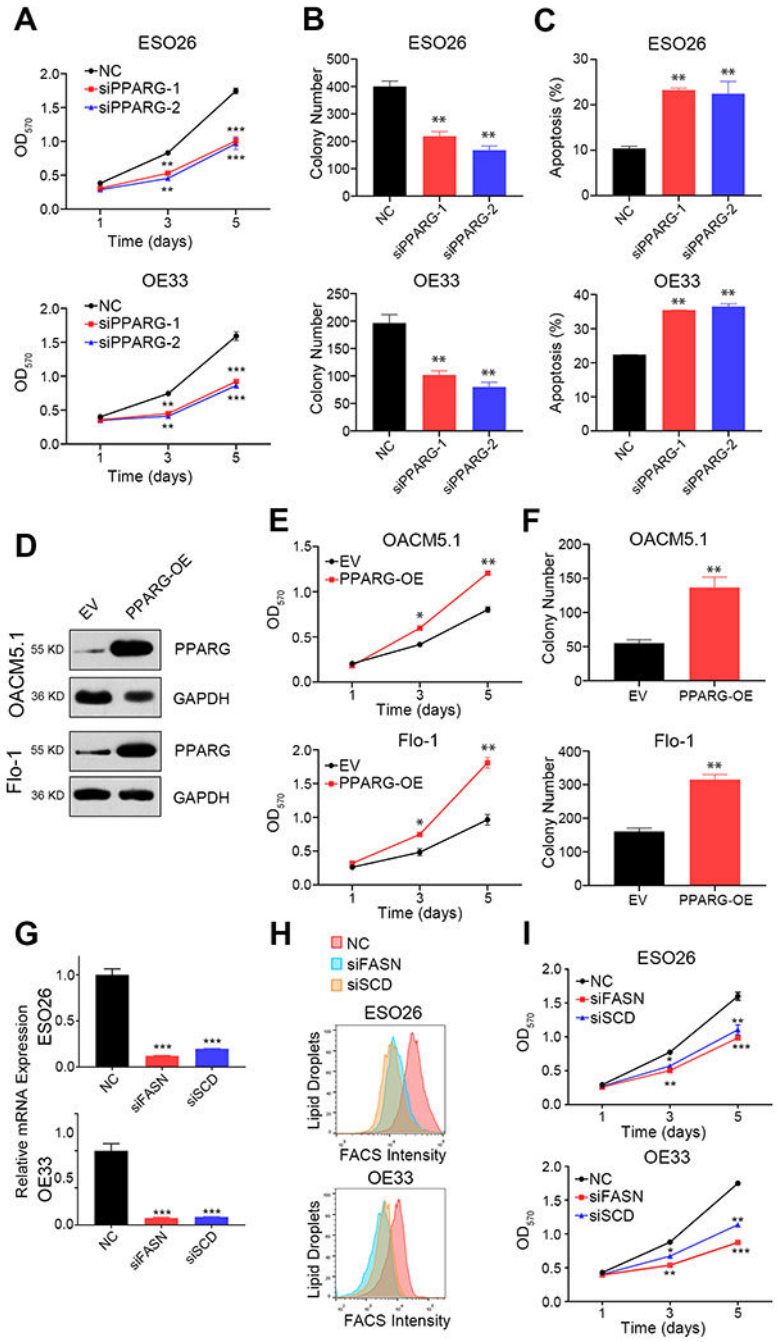

Figure 4. Inhibition of PPARG/fatty-acid synthesis pathway suppresses EAC cell viability

Knockdown of PPARG by individual siRNAs inhibited (A) cell proliferation and (B) colony growth, while (C) increased cell apoptosis in different EAC cell lines. (D) PPARG was overexpressed and verified by Western blotting in different EAC cell lines. (E) Overexpressed (OE) PPARG promoted cell proliferation and (F) colony growth compared with empty vector control (EV). (G) Knockdown of either FASN or SCD decreased lipid droplet (H) and cell proliferation (I). Mean±SD are shown, n=3. *, $p<0.05$; **, $p<0.01$;***, $p<0.001$.

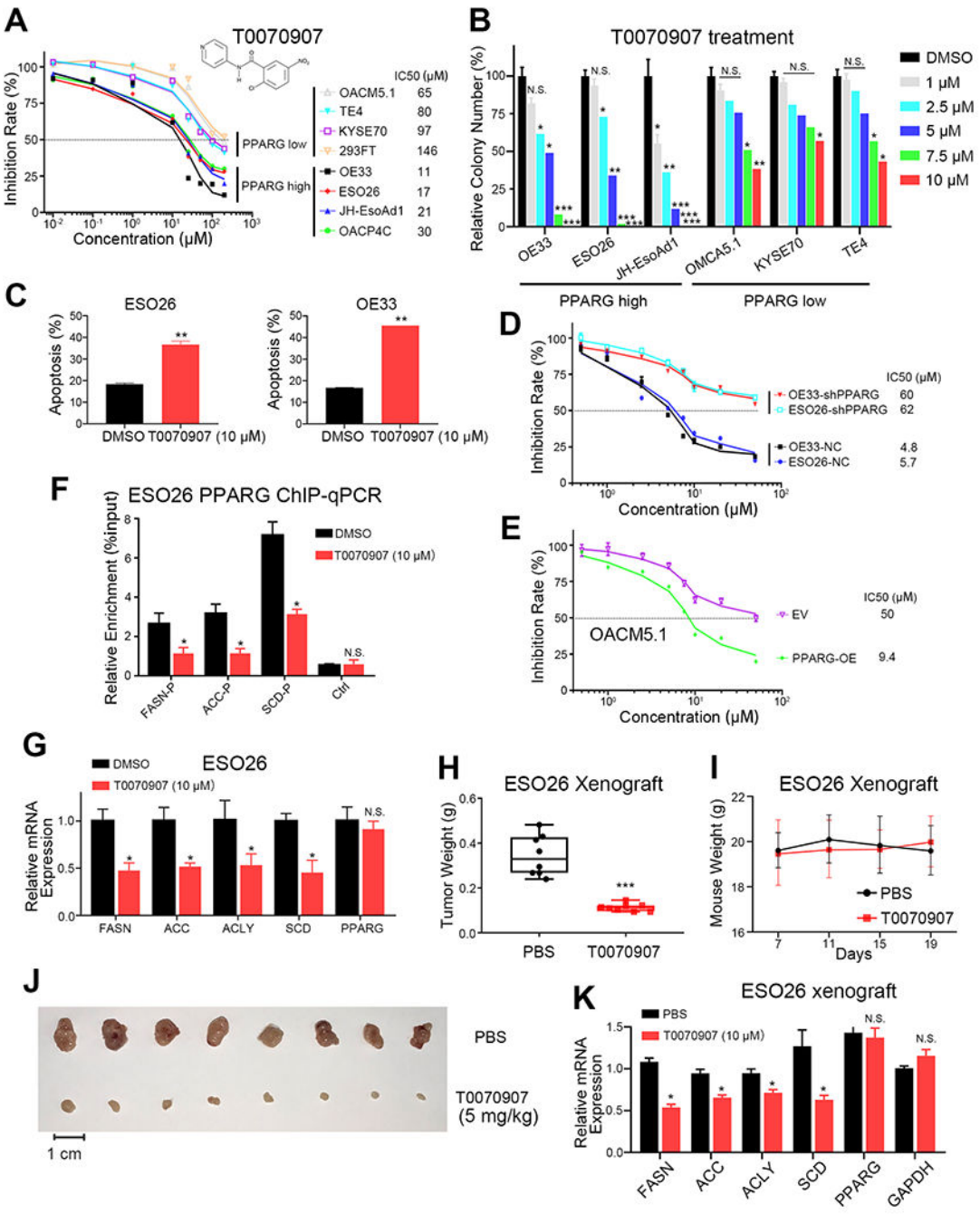

Figure 5. T0070907, a PPARG-specific inhibitor, shows potent anti-EAC function

(A) Short-term cell viability assay measuring the IC50s of T0070907 in different cell lines. (B) Relative number of colonies formed at different concentrations of T0070907. (C) Treatment of T0070907 increased cell apoptosis. (D) Short-term cell viability assays measuring T0070907 IC50s in either (D) PPARG knockdown or (E) over-expression cells. (F) ChIP-PCR using PPARG antibody either with or without T0070907 treatment. (G) mRNA levels of PPARG-target genes after T0070907 treatment. (H) Xenograft weight, (I)

mouse weight, (J) xenograft photos, and (K) gene expression from indicated groups. Mean ±SD are shown, n=3. *, $p<0.05$; **, $p<0.01$; ***, $p<0.001$; N.S., not significant.

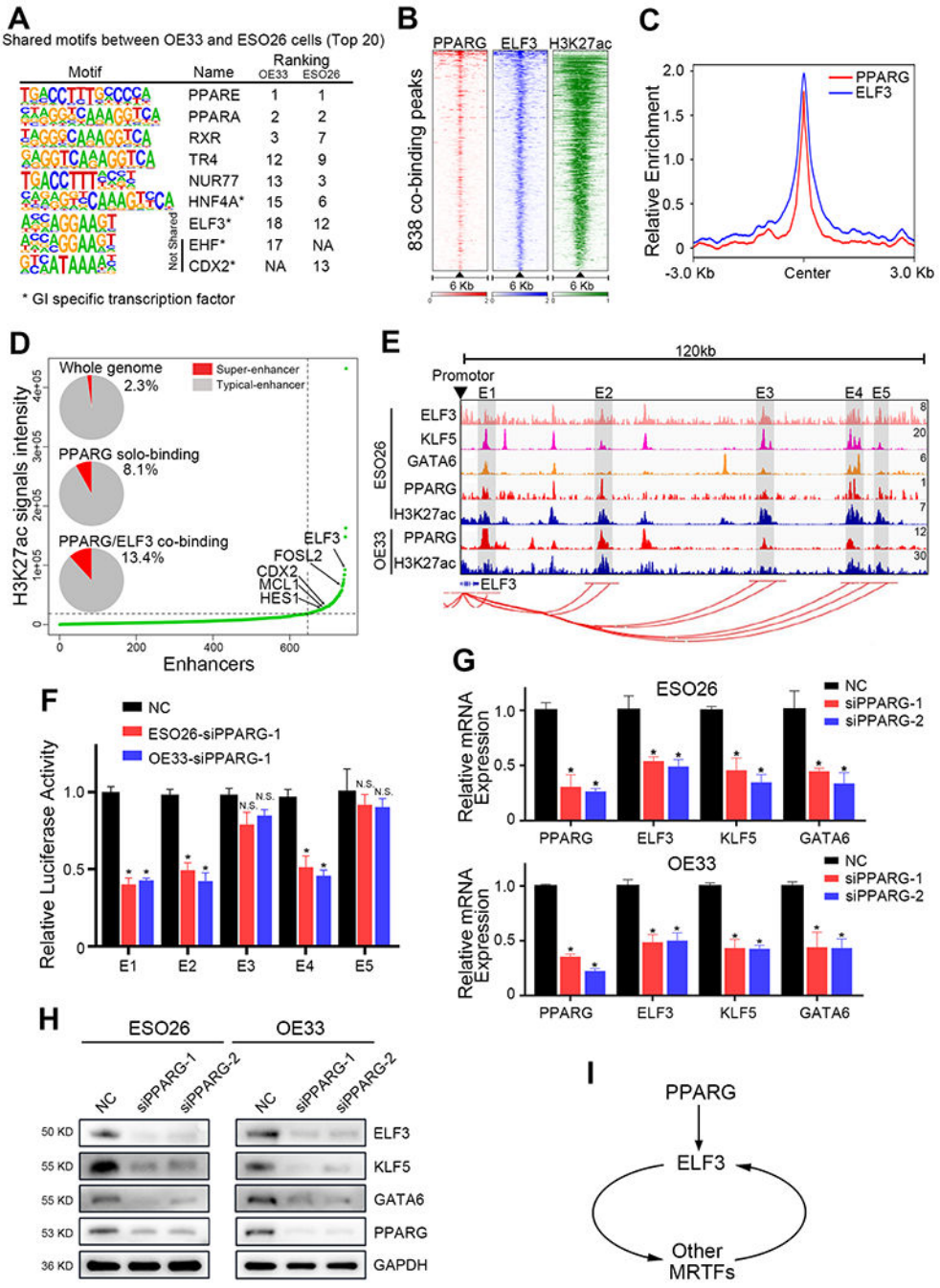

Figure 6. PPARG cooperates with ELF3 and directly co-activates ELF3 super-enhancer

(A) Top enriched motifs of PPARG ChIP-Seq shared in ESO26 and OE33 cells. Note that EHF and CDX2 are not overlapped. (B) Heatmap showing ChIP-Seq signals at PPARG/ELF3 co-binding regions, ordered by the intensity of PPARG peaks. Lines, peaks. (C) Line plots showing the distribution of PPARG/ELF3 ChIP-Seq signals in their co-binding regions. (D) Inflection plot ranking all enhancers co-occupied by PPARG/ELF3. Pie charts showing the percentage of super-enhancers and typical-enhancers. (E) IGV plots of H3K27ac and TF ChIP-Seq signals in ESO26 and OE33 cells. Connecting lines show enhancer-promoter

interactions detected by 4C as we published recently(5). (F) Enhancer activity measured by luciferase reporter assays. (G) mRNA levels of MRTFs after siRNA knockdown of PPARG. (H) Western blot of indicated proteins upon PPARG knockdown. (I) Schematic graph of the regulatory relationship between PPARG and MRTFs summarized from Figure 6. Mean±SD are shown; n=3. *, $p<0.05$; N.S., not significant.

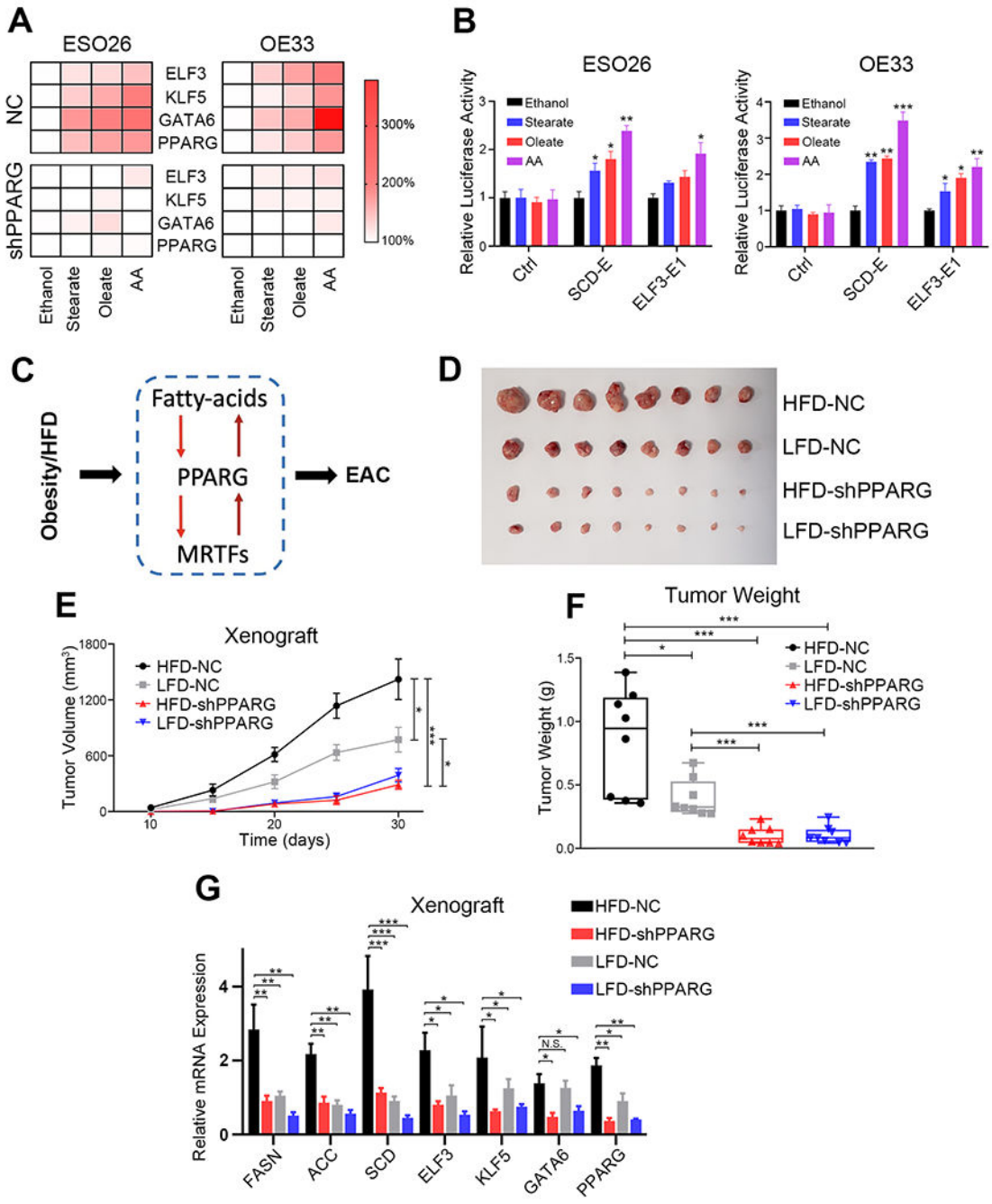

Figure 7. A transcriptional feedback loop of Fatty-acid/PPARG/MRTF in EAC

(A) Heatmap of fold changes of MRTF mRNA levels (B) and enhancer activity measured by luciferase assays following treatment with different fatty-acids (10 μM) for 48h. (C) Schematic diagram of a transcriptional feedback loop involving fatty-acid/PPARG/MRTF in EAC. (D) Xenograft images, (E) growth curves and (F) tumor weights of xenograft expressing either scramble shRNA or PPARG-shRNA which were grown in mice fed with either high-fat diet (HFD) or low-fat diet (LFD). (G) mRNA levels of indicated genes were

measured by qRT-PCR. Mean±SD are shown, n=3 *, p<0.05; **, p<0.01; ***, p<0.001; N.S., not significant.